High latitude vegetation changes will determine future plant volatile impacts on atmospheric organic aerosols

Jing Tang (jing.tang@nateko.lu.se)
Lund University
Putian Zhou
University of Helsinki
Paul Miller
Lund University
Guy Schurgers
University of Copenhagen https://orcid.org/0000-0002-2189-1995
Adrian Gustafson
Lund University
Risto Makkonen
Finnish Meteorological Institute
Yongshuo Fu
Beijing Normal University
Riikka Rinnan
University of Copenhagen https://orcid.org/0000-0001-7222-700X

Article

Keywords:

Posted Date: December 9th, 2021

DOI: https://doi.org/10.21203/rs.3.rs-1143422/v1

High latitude vegetation changes will determine future plant volatile impacts on atmospheric organic aerosols

Jing Tang[1,2,3*], Putian Zhou[4], Paul A. Miller[1], Guy Schurgers[3,5], Adrian Gustafson[1,6], Risto Makkonen[4,7], Yongshuo H. Fu[8], Riikka Rinnan[2,3].

[1.] Department of Physical Geography and Ecosystem Science, Lund University, Sölvegatan 12, SE-223 62, Lund, Sweden

[2.] Terrestrial Ecology Section, Department of Biology, , Universitetsparken 15, DK-2100, Copenhagen Ø, Denmark

[3.] Center for Permafrost (CENPERM), University of Copenhagen, Øster Voldgade 10, DK-1350, Copenhagen K, Denmark

[4.] Institute for Atmospheric and Earth Systems Research/Physics, University of Helsinki, 00014, Helsinki, Finland

[5.] Department of Geosciences and Natural Resource Management, University of Copenhagen, Copenhagen, Denmark

[6.] Center for Environmental and Climate Science, Lund University, Sölvegatan 37, 223 62, Lund, Sweden

[7.] Climate System Research, Finnish Meteorological Institute, Helsinki, Finland

[8.] College of Water Sciences, Beijing Normal University, Beijing, China

Contacting author: Jing Tang (jing.tang@nateko.lu.se)

Abstract

Strong, ongoing high latitude-warming is causing changes to vegetation composition and plant productivity, modifying plant emissions of Biogenic Volatile Organic Compounds (BVOCs). In the sparsely populated high latitudes, climatic feedbacks resulting from BVOCs as precursors of atmospheric aerosols could be more important than elsewhere on the globe. Here, we quantitatively assess the linkages between vegetation changes, BVOC emissions and secondary organic aerosol (SOA) under different climate scenarios and show that warming-induced vegetation changes determine the spatial patterns of BVOC impacts on SOA. The northward advances of boreal needle-leaved trees and shrubs result in an increase of up to 45% in regional SOA optical depth, causing a cooling feedback. In contrast, areas dominated by temperate broad-leaved trees show a large decline in monoterpene emissions and SOA formation, causing a warming feedback. We highlight the necessity of considering vegetation shifts when assessing radiative feedbacks on climate following the BVOC-SOA pathway.

Main

The northern high latitudes are experiencing stronger warming than the global average and this warming is reflected in observed changes to vegetation composition, plant traits and plant productivity[1,2], which could profoundly alter the magnitude and composition of plant-emitted Biogenic Volatile Organic Compounds (BVOCs)[3]. Warming-induced permafrost thaw could release previously-locked nutrients, abating nutrient limitations and thereby supporting enhanced plant productivity and growth in this region[4,5]. The predicted increase of atmospheric CO_2 concentration might, however, inhibit BVOC production as has been experimentally shown for isoprene synthesis under elevated CO_2[6,7]. However, it remains unclear how the BVOC emissions might respond to the fast and combined environmental changes in the high latitudes.

Plant-emitted BVOCs participate in a series of chemical reactions in the atmosphere, which influences atmospheric oxidation capacity[8], tropospheric ozone concentrations[9], and increase the concentrations of secondary organic aerosol (SOA) and cloud condensation nuclei (CCN)[10,11]. In the high latitude atmosphere, the anthropogenic sources of aerosols and CCN are generally lower than in denser inhabited regions[12,13]. Thus, the warming-induced vegetation changes and the following alterations in BVOC emissions may provide stronger

feedbacks to the high latitude climate system through modulating atmospheric SOA and CCN concentrations than elsewhere on the globe. Despite this, the biochemical and biophysical BVOC-mediated feedbacks to the climate have been largely ignored in the high latitudes[12]. Furthermore, previous estimates of high latitude BVOC emissions are highly uncertain[14,15] due to the scarcity of observation-based emission data and/or underrepresented plant variations in large-scale modelling, particularly in the tundra biome[3]. Here, we quantitatively assess future BVOC dynamics in the Arctic and boreal regions, elucidate key processes driving the trends in BVOC emissions and illustrate the contribution of BVOC emissions to our climate system through SOA-CCN-climate feedbacks.

Future changes in isoprene and monoterpene emissions

We explore both historical and future emission changes of the dominant BVOCs, isoprene and monoterpenes, using a dynamic vegetation model, LPJ-GUESS[16]. The model, driven by climate data, simulates plant competition and vegetation composition change, as well as plant and soil biochemical processes in response to changing environmental conditions (Methods). Observation-based BVOC emission rates and temperature response curves, together with a detailed representation of tundra plant functional types (PFTs) have allowed to simulate BVOC emissions for the Arctic area[3,17]. Details of model evaluations over different historical periods can be found in the Extended Data Figs 1-3 and Extended Data Table 1.

For the future period (2015-2100), we select climate projections from three General Circulation Models (GCMs) following five different Shared Socioeconomic Pathways (SSPs) under the CMIP6 framework[18] and implement bias-correction of these climate predictions of temperature, precipitation and radiation before using them to drive LPJ-GUESS (Methods). The resulting 15 scenarios (see overview of the scenarios in Extended Data Table 2 and future anomalies of temperature, precipitation and radiation in the Extended Data Fig. 4) represent SSPs with varying greenhouse gas projections and GCMs with different climate sensitivities in the study region (tundra and boreal biomes based on RESOLVE ecoregions2017[19]). We use the LPJ-GUESS outputs driven by these 15 climate projections (hereafter standard runs) to explore future BVOC emissions.

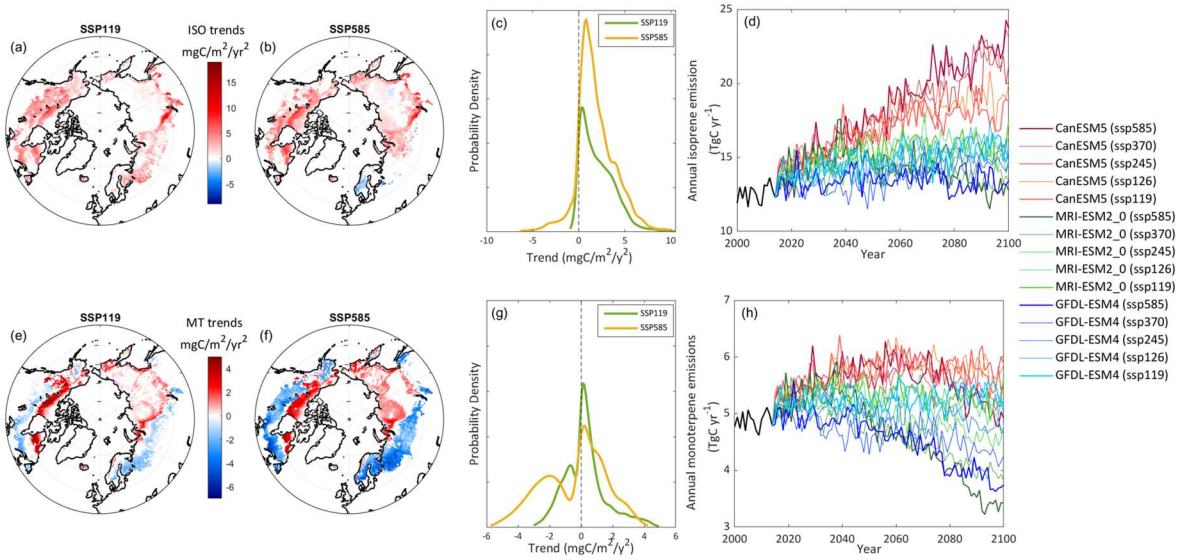

Figure 1. LPJ-GUESS modelled trends of isoprene and monoterpene emissions for the period of 2001-2100. (a-b): Modelled isoprene (ISO) trends for SSP119 and SSP585, respectively. The trends are analysed based on the averaged emissions over 3 General Circulation Models (GCMs) and only significant trends (Mann-Kendall trend test, $p<0.05$) are shown; (c) Probability density function of significant trends in isoprene emission; (d) Time series of areal total isoprene emissions for all standard runs driven by 3 GCMs following 5 SSPs; (e-f): Modelled monoterpene (MT) trends for SSP119 and SSP585, respectively. The trends are analysed based on the averaged emissions over 3 GCMs and only significant trends (Mann-Kendall trend test, $p<0.05$) are shown; (g) Probability density function of significant trends in monoterpene emissions; (h) Time series of areal total monoterpene emissions for all standard runs driven by 3 different GCMs following 5 SSPs. SSP119: Shared Socioeconomic Pathway 1 reaching radiative forcing of 1.9 W/m^2 in 2100. SSP585: Shared Socioeconomic Pathway 5 reaching radiative forcing of 5.8 W/m^2 in 2100.

We simulate a clear increase in the areal total of annual isoprene (increase by 74-120% by the 2100) and monoterpene (11-36% by the 2100) emissions for the runs driven by CanESM5 under different SSPs (Fig. 1d, 1h). For the simulations driven by scenarios combining a more moderate temperature increase with high CO_2 concentration (such as MRI-ESM2_0 SSP585 and GFDL-ESM4 SSP585, see temperature anomalies in Extended Data Fig. 4a), the total isoprene emissions show moderate increases and the total monoterpene emissions show clear decreases (Fig. 1h).

Spatially, isoprene emissions significantly increase in many regions, with the largest increasing trends simulated in regions where the dominant PFTs shift strongly (Fig. 2). The projected shifts include the replacement of boreal needle-leaved evergreen trees with broad-leaved deciduous trees (shift from PFT BNE to PFT IBS in Fig. 2) in northern Canada and western Russia, and a northward movement of boreal needle-leaved evergreen trees replacing herbaceous vegetation and shrubs in eastern Russia, Alaska and north-eastern Canada (See BNE in these regions in Fig. 2b-e). In the High Arctic, shrub abundance increases strongly, especially under CanESM5 SSP585 (See HSS in Fig. 2 and latitudinal fractions of each PFT in Extended Data Fig. 6b). These modelled PFT

shifts are in agreement with predictions based on different approaches[20,21] and consistent with paleo-records of warm periods[22].

Compared with the increasing trends under SSP119, the modelled isoprene emissions under SSP585 in Scandinavia show decreasing trends, which might be linked to the strong CO_2 inhibition of isoprene production[23], since the atmospheric CO_2 concentrations reach up to 1100 ppm by the end of the 21st century. For monoterpenes, the largest increasing trends occur in northern Canada and Russia (mainly for SSP585), where boreal needle-leaved evergreen (in Canada) and needle-leaved deciduous (in Russia) trees with relatively high emission capacities replace the isoprene-emitting grass PFT in the simulations. In the southernmost study regions, we observe a clear decrease in monoterpene emissions, especially under SSP585 (Fig. 1f), as the widespread broad-leaved, isoprene-emitting, deciduous trees replace monoterpene-emitting boreal needle-leaved trees. These unfavourable vegetation shifts for monoterpenes accompany with high atmospheric CO_2 increase in this climate prediction. In general, the predicted changes in isoprene and monoterpene emissions vary among climate scenarios, in agreement with global studies[24], and show regionally varying responses linked to the shifts of dominant vegetation.

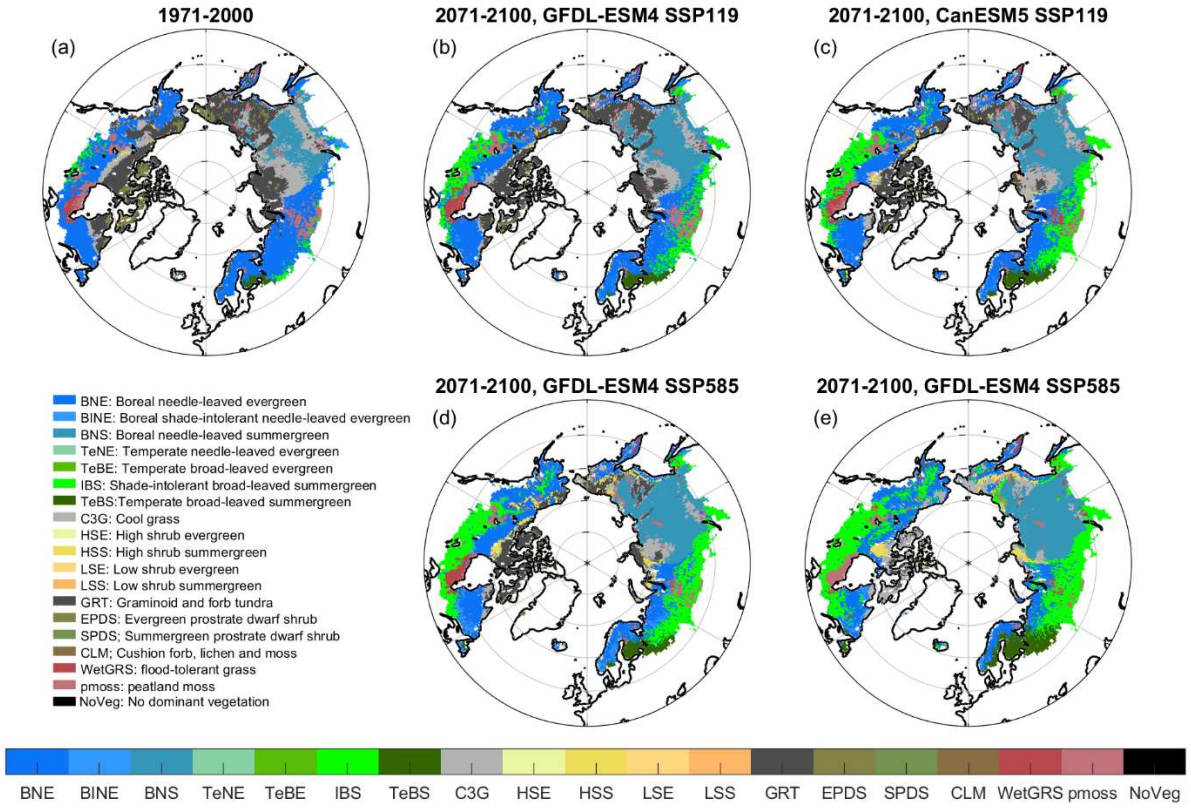

Figure 2. Distribution of the dominant plant functional types (PFTs) over the period 1971-2000 (a) and 2071-2100 (b-e) based on the modelled leaf area index. The outputs from the scenario SSP119 are shown in b-c, and the outputs from SSP585 are shown in d-e. The outputs from two GCMs are plotted separately: GFDL-ESM4 (b,d),and CanESM5 (c,e).

Key processes regulating future BVOC trends

Changing temperature and atmospheric CO_2 concentration can exert direct impacts on BVOC synthesis[6-8]. On top of that, syntheses of isoprene and monoterpenes are linked to plant photosynthesis[23,25,26]. Atmospheric CO_2 concentration, soil nitrogen availability as well as climate conditions not only alter photosynthetic rates, but also vegetation dynamics, including plant growth and competition, migration as well as mortality, indirectly influencing BVOC emission magnitudes and composition. In this study, we investigate the following four drivers: climate, vegetation changes, atmospheric CO_2 concentration, and nitrogen (N) availability, and run different factorial simulations based on CanESM5 SSP119 and SSP585. We design four factorial experiments: (1) constant CO_2 concentration at year 2014 level for the future period (hereafter noCO2); (2) setting CO_2 inhibition impacts on BVOC production as in 2014 (noCO2Inhibition); (3) adding 50 kg N/ha/yr to annual nitrogen deposition to reduce nitrogen limitation (noNlim). This N addition corresponds to what has been implemented in forest N fertilization trials in Davies-Barnard, et al. [27]; (4) using the monthly averages of climate drivers from the period 2005-2014 for driving ecosystem processes, but keeping the predicted future climate for BVOC synthesis in the model for the future period 2015-2100 (noVegDym). Subsequently, we calculate the differences between the standard and factorial simulations (Extended Data Table 3) to tease apart the relative importance of CO_2 fertilization, CO_2 inhibition of BVOC production, N limitation and vegetation changes as determinants of spatial and temporal patterns of future BVOC emissions (Fig. 3).

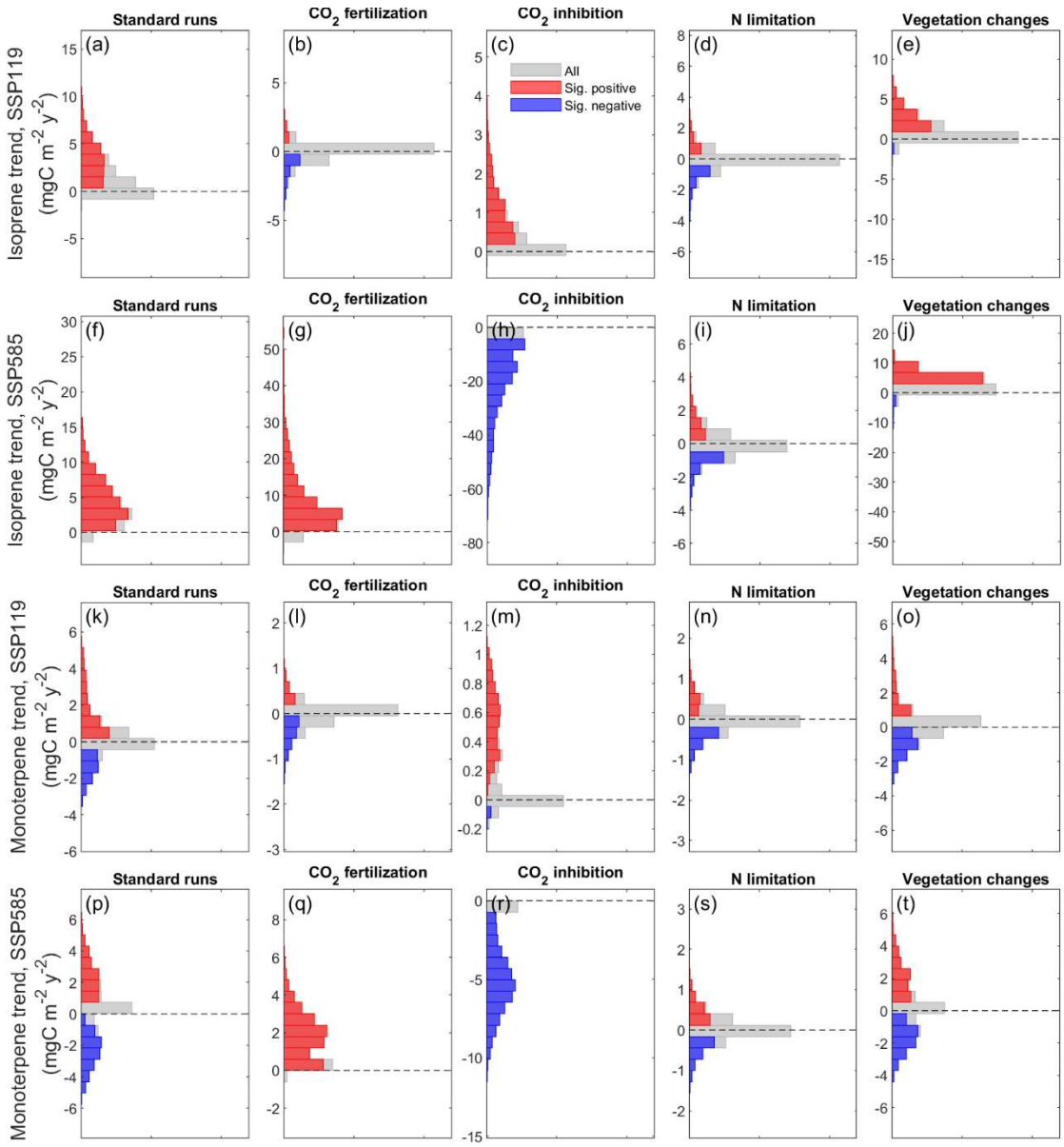

129

130 *Figure 3 Histograms of trends in modelled isoprene (first row for CanESM5 SSP119, and second row for CanESM5 SSP585)*
131 *and monoterpene (third row for CanESM5 SSP119, and fourth row for CanESM5 SSP585) emissions from standard runs and*
132 *from four investigated processes. Trends are analysed using Mann-Kendall test, and both significant positive and significant*
133 *negative trends ($p < 0.05$) are marked on as red and blue bars, respectively. Please note the change of scales on the y-axes.*
134 *Sig.: Significant.*

135

136 We find that under the low CO_2 emission scenario (CanESM5 SSP119), the overall positive trend in isoprene
137 emissions is largely driven by vegetation changes (Fig. 3a, e). The small increasing emission trends by CO_2
138 inhibition in both isoprene and monoterpene emissions are driven by decreasing atmospheric CO_2 concentrations
139 towards the end of the century (see CO_2 inhibition in Fig. 3c, m). Overall, the impacts from CO_2 fertilization and
140 N limitation are rather limited for both isoprene and monoterpenes under CanESM5 SSP119 (Fig. 3b, d, l, n).

Under the high CO_2 emission scenario (CanESM5 SSP585) with associated stronger warming and large increases in N deposition, the positive trends in isoprene emissions are associated with CO_2 fertilization of photosynthesis and vegetation changes but are simultaneously negatively influenced by CO_2 inhibition of BVOC production (Fig. 3g, h, j). Climate warming-induced vegetation changes promote the overall positive trend in isoprene (Fig. 3j), but not in monoterpene emissions, as depicted by the interplay between positive and negative impacts under CanESM5 SSP585 (Fig. 3t). The impacts from N limitation are again very small, likely linked to the increased N deposition during this century in CanESM5 SSP585 and increased sources of mineral N from warming soils (data not shown here).

BVOC impacts on regional atmosphere

The modelled BVOC emissions, together with vegetation status (including leaf area index, LAI and vegetation cover fraction) of the years 2009 and 2100 from standard runs driven by CanESM5 SSP119 and CanESM5 SSP585 are fed into the global chemistry transport model version 5 (TM5, Bergman, et al. [28]) to quantify the impacts of isoprene and monoterpene emissions on surface SOA concentrations (SOA_{surf}), SOA optical depths at 550 nm ($OD550_{SOA}$) and aerosol optical depths at 550 nm ($OD550_{aer}$). The outputs from two of the factorial experiments that contribute most to the simulated BVOC trends (Fig 3, noCO2inhibition and noVegDym) (Fig. 3) driven by CanESM5 SSP585 and CanESM5 SSP119 are also used as inputs for TM5 (see Methods for the detailed setup for TM5).

Our results demonstrate the important role of climate change-driven vegetation changes in regulating the spatial patterns of BVOC impacts on regional atmospheric aerosols. The increased BVOC emissions have largely contributed to the increase in surface concentration of SOA (SOA_{surf}) for a major part of the study region, with a smaller area of increase for CanESM5 SSP119 than for CanESM5 SSP585 (Fig. 4g & Fig. 5g). Under both SSP scenarios, we see an up to 2.7-fold increase of SOA_{surf} in northern Canada and Russia in the standard run. The simulation without vegetation responses to climate change (noVegDym) depicts a considerably lower increase (Fig. 4h and Fig. 5h). The standard runs with vegetation changes show stronger and vaster increases in aerosol optical depth ($OD550_{SOA}$ and $OD550_{aer}$, 41% and 4.9% increase under CanESM5 SSP119, Fig. 4 j&m, and 29 % and 4.1% increase under CanESM5 SSP585, Fig. 5 j&m, respectively). Without vegetation changes (noVegDym), only a limited increase of $OD550_{SOA}$ and $OD550_{aer}$ in a small region in the central and eastern Canada is simulated. The strong spatial linkages, which we show for vegetation shifts, BVOC dynamics and SOA/aerosol changes are ignored when using static vegetation distributions for future conditions[14]. Under the

warmest scenario (i.e., CanESM5 SSP585), the widespread replacement of boreal needle-leaved trees with broad-leaved deciduous trees (Fig. 2e) in Sweden and Finland clearly contributes to the reduction of SOA_{surf} and optical depths (Fig. 5 g, j, m). When future CO_2 inhibition of BVOC production is excluded, TM5 estimates up to 10-fold increases of SOA_{surf} (mainly in the high latitudes), up to a 1.2-fold increase of $OD550_{SOA}$, and up to an 18% increase in $OD550_{aer}$ in the year 2100 as compared to 2009 under CanESM5 SSP585. Similar patterns but with slightly smaller magnitudes are observed when CO_2 inhibition is only excluded for monoterpenes (data not shown). Under SSP119, the effects of atmospheric CO_2 on regional SOA and aerosols via BVOCs are limited. Our results emphasizes the importance of monoterpenes in influencing SOA and aerosol yields[28], and shows that we need to understand whether CO_2 inhibition affects monoterpene production in high latitude plants similarly to those studied plants[6,7,29].

The simulated changes in BVOCs and SOA lead to increases of CCN concentration at supersaturation of 1% near the surface mainly for the Arctic region (Extended Data Fig. 7), which indicates potential enhanced formation of low-level clouds. For example, without CO_2 inhibition under CanESM5 SSP585, CCN over Greenland and eastern Canada increases by 16 % (Extended Data Fig. 7c). The increased cover of low-level clouds can have both warming (re-emitting received longwave radiation from the ground) and cooling (scattering and reflecting shortwave radiation) feedbacks on the climate[12]. The net radiative impacts from BVOC changes in high latitudes are not accounted for in TM5 and therefore not evaluated in this study.

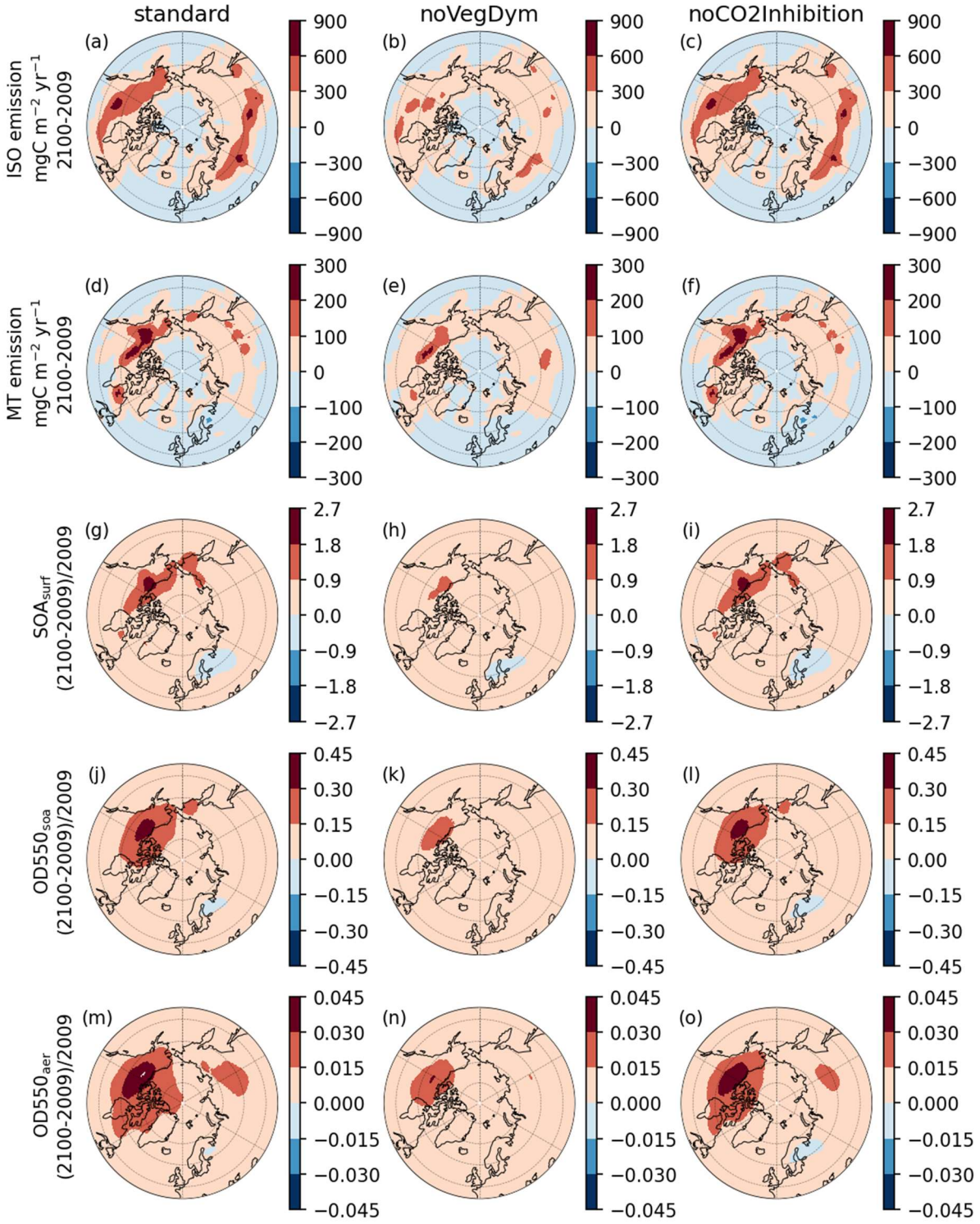

Figure 4 The inputs to and outputs from TM5 using CanESM5 SSP119. The first and second rows show LPJ-GUESS simulated isoprene (ISO) and monoterpene (MT) emission changes between 2100 and 2009. The emissions from the year 2100 are driven by CanESM5 SSP119. The third to the fifth rows show the TM5 simulated ratio in changes to surface SOA concentration (SOA_{surf}); optical depth of SOA at 550 nm ($OD550_{soa}$); and optical depth of aerosol at 550 nm ($OD550_{aer}$). From left to right, we show the TM5 results fed with BVOC inputs from three LPJ-GUESS runs, which are standard run (the 1st column), noVegDym run (the 2nd column) and noCO2Inhibition run (the 3rd column). The colour bars used for these three columns are kept the same for each corresponding output.

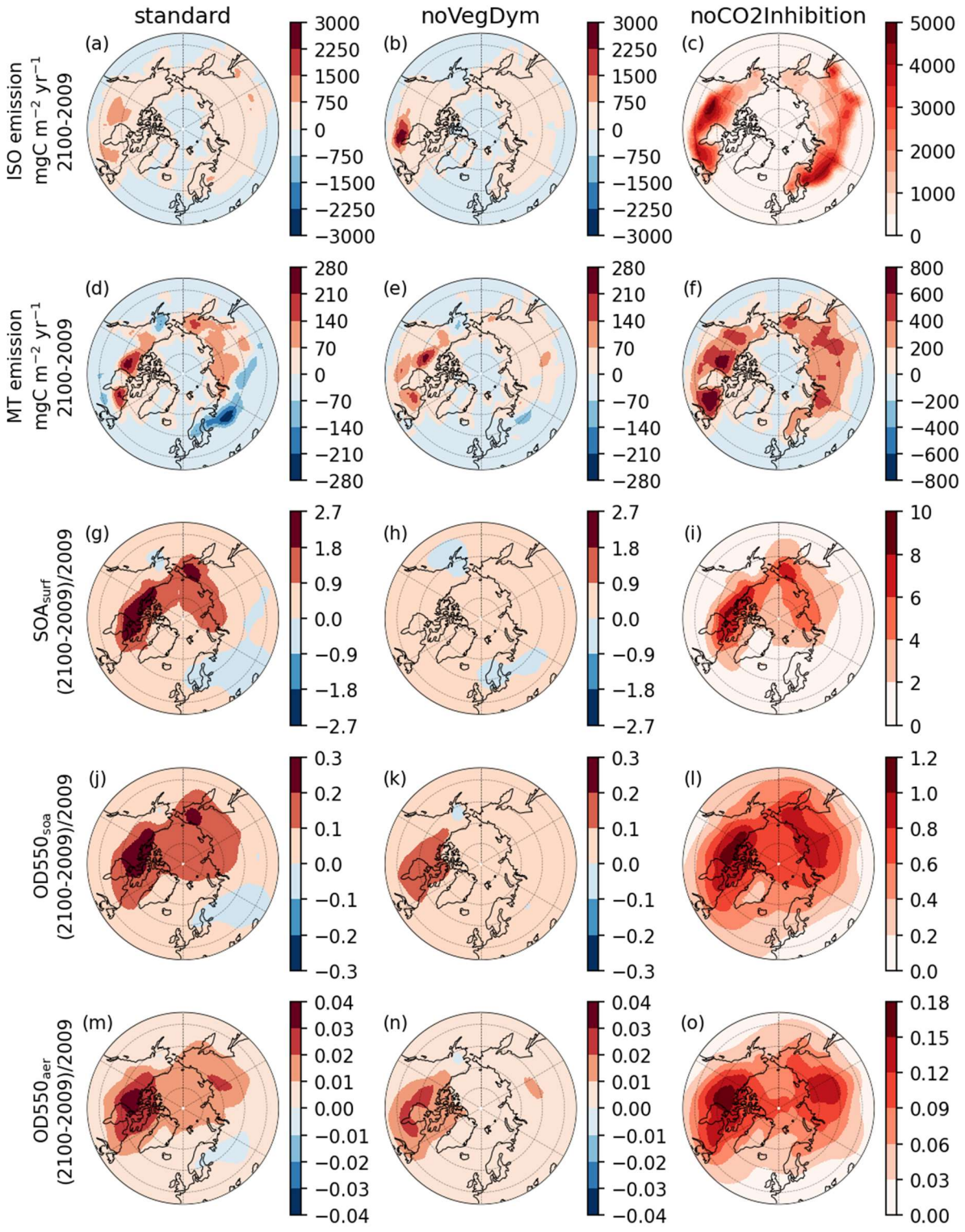

Figure 5 The inputs to and outputs from TM5 using CanESM5 SSP585. The first and second rows show LPJ-GUESS simulated isoprene (ISO) and monoterpene (MT) emission changes between 2100 and 2009. The emissions from the year 2100 are driven by CanESM5 SSP585. The third to the fifth rows show the TM5 simulated ratio in changes to surface SOA concentration (SOA_{surf}); optical depth of SOA at 550 nm ($OD550_{soa}$); and optical depth of aerosol at 550 nm ($OD550_{aer}$). From left to right, we show the TM5 results fed with BVOC inputs from three LPJ-GUESS runs, which are standard run (the 1st column), noVegDym run (the 2nd column) and noCO2Inhibition run (the 3rd column). The colour bars used for standard and noVegDym runs are kept the same for each corresponding output.

Discussion and conclusions

Our results illustrate that vegetation changes in a warmer climate play a crucial role in shaping future BVOC feedbacks to atmospheric chemistry and climate. Previous assessments of feedbacks between the land surface and the atmosphere in high latitudes that involve vegetation changes have focused on changes in surface albedo[20,30], and increases in atmospheric water vapour[31], but our study clearly demonstrates the strong and regionally diverse feedbacks of vegetation changes on our climate through the BVOC-SOA pathway. The warming-induced and widespread increase of broadleaved deciduous trees at the expense of boreal evergreen needle-leaved trees in the boreal region suppressed the emissions of monoterpenes and thereby SOA formation, causing a regional warming feedback. In the Arctic, the increased abundance of shrubs and the northward advance of boreal needle-leaved trees in northern Canada and Siberia greatly contributed to an increase of surface SOA, resulting in up to 45% increase in SOA optical depth and likely leading to cooling feedback to our climate. Currently, the Arctic features a lack of aerosol particles for cloud formation[13], and the northward shifts of vegetation bring in a new, important aerosol source: plant-emitted BVOCs. This 'new' source of aerosols might enhance cloud formation in this region. During the growing season, the enhanced cloud coverage might lead to cooling feedbacks through scattering shortwave radiation greater than warming feedbacks associated with re-emission of longwave radiation received from the land surface[13]. The overall net feedbacks from the vegetation-BVOC-SOA pathway on our climate need to be comprehensively evaluated considering the negative feedbacks from scattering and cloud formation from SOA, and also the positive feedbacks from increased longwave radiation emitted from low-level clouds[12].

Under high CO_2 emission scenarios, the climate warming-induced increase of natural aerosols from plant BVOC emissions is largely constrained by CO_2 inhibition of BVOC (mainly monoterpene) production, which means that future anthropogenic CO_2 increase might provide an indirect positive feedback to the climate through this inhibition. Young et al. [32] showed that the inhibition of isoprene production by the future CO_2 increases can, via atmospheric oxidation, increase hydroxyl radical (OH) concentrations, which can decrease the lifetime of methane by 7 months. The potential for strong atmospheric feedbacks associated with plant BVOC responses to the increasing atmospheric CO_2 concentrations make urgent the need for more leaf- and ecosystem-level observations to unveil the mechanisms for the decoupling between photosynthesis and BVOC production under elevated CO_2. Furthermore, it is still unclear whether elevated CO_2 inhibits monoterpene production to the same degree as isoprene production. The empirical function used in LPJ-GUESS to assess the CO_2 impact on terpenoid production[23] was derived from a limited number of observation studies on trees. Whether the BVOC

emissions of low-statured Arctic plants respond similarly to CO_2 is unknown. We currently have no published data that enable a quantification of the low-statured plants' BVOC responses to the surrounding CO_2.

Because the current TM5 simulation settings neither consider the impacts from future changes in meteorology, nor other surface emissions except isoprene and monoterpenes, the current TM5 setup allows us to single out the 'isolated' impacts from plant-emitted isoprene and monoterpenes alone, regardless of interactions with future changes in other factors (see "Model uncertainties" in Extended Data). Future studies should focus on quantification of the synergistic effects of future plant emissions from high latitudes with other anthropogenic and primary aerosol sources in a coupled Earth System Model (such as [33]).

Our results show a potentially significant feedback mechanism linking climate change-induced vegetation composition changes, BVOC dynamics and aerosols in the high latitudes. The negative feedback mechanism between the biosphere, aerosols, and climate concluded from observation data[10] cannot be extrapolated into the future without considering climate change-induced vegetation changes and their impacts on emitted compounds. Our study confirms the importance of BVOCs for future atmospheric SOA concentration and optical depths in the high latitudes. It also reveals the overall impacts largely depend on how atmospheric CO_2 concentration influences monoterpene production. The net radiative feedbacks from BVOCs need a comprehensive evaluation in order to assess the balance between aerosol shortwave cooling and aerosol longwave warming feedbacks in the high latitude environment.

Materials and methods

Dynamic vegetation model, LPJ-GUESS

We used the latest version of LPJ-GUESS v4.1 with the relevant developments of wetland biogeochemistry and soil physics following[34,35]. LPJ-GUESS is a dynamic ecosystem model, which simulates vegetation growth, mortality, and competition, as well as soil biogeochemistry[16]. The model has been widely used to assess water, nitrogen and carbon fluxes, as well as vegetation dynamics at regional and global scales. Plants are represented as plant functional types (PFTs) with a set of predefined bioclimatic, physiological, life history and phenological parameters that characterize specific plant growing requirements and spatial distribution. For simulations in high latitudes, different levels of shrubs (high, low and prostrate), lichen, moss and wetland PFTs are specified[17]. Compared with the version of LPJ-GUESS described in Smith et al.,[16], the model version used here includes improved soil temperature calculations, allowing a better representation of soil thawing and freezing processes and influencing water availability to plants. The model also includes wetland biogeochemistry and wetland

hydrology [36].

Daily leaf-level photosynthesis is based on the simplified version of the Farquhar biochemical model[37,38], which simulates a gradual transition between an electron-transport-limited and a rubisco-limited carbon assimilation. In the model, a fraction of the photosynthetic electron flux is used to produce isoprene[23] and monoterpenes[25], and the production rates of isoprene and monoterpenes are also influenced by PFT-specific emission factors, leaf temperature, seasonality and atmospheric CO_2 concentration. The PFT-specific emission factors (standardized emission rates at photosynthetically active radiation levels of 1000 μmol/m^2/s and at a reference temperature of 20 °C for Arctic PFTs) in the tundra region are based on the branch- or leaf-level measurement data (see details in[3,17]), and a stronger temperature sensitivity derived in Tang, et al. [17] has been applied for Arctic PFTs. For boreal and temperate PFTs, the global temperature response curve has been used and the emission factors are based on the reference temperature of 30 °C.

Standard runs

For simulation of the historical period in this study, we used the monthly CRU-NCEP climate data[39] for the period of 1901-2014, and the detrended CRU-NCEP temperature, precipitation and radiation data over 1901-1930 were repeatedly used for the period 1850-1900. For the future period (i.e., 2015-2100), we selected the climate outputs from three general circulation models (GCMs), each following five different Shared Socioeconomic Pathways (SSPs) from the latest CMIP6 project[18] to represent a range of predicted future climates. The three GCMs were selected based on our analysis of temperature changes in the high latitudes, and also on the completeness of the published outputs of these five SSPs (as the dates of access in September 2020) to represent a wide range of future temperature changes in the study region. The monthly climate data from each GCM and SSP for the future period were bias corrected. The biases were calculated as the difference between the monthly climate data of the period 1985-2014 from CRU-NCEP and climate outputs from each scenario in the same period, and these biases were then added to the future climate simulated by the GCM. A detailed description of the bias-correction approach can be found in Ahlström, et al. [40]. The predicted anomalies in future temperature, precipitation, and radiation for the 15 scenarios (3 GCMs x 5 SSPs) are presented in Extended Data Fig. 4. All 15 standard runs share a common climate development during the historical period and start to diverge from 2015 onwards following the different future predictions.

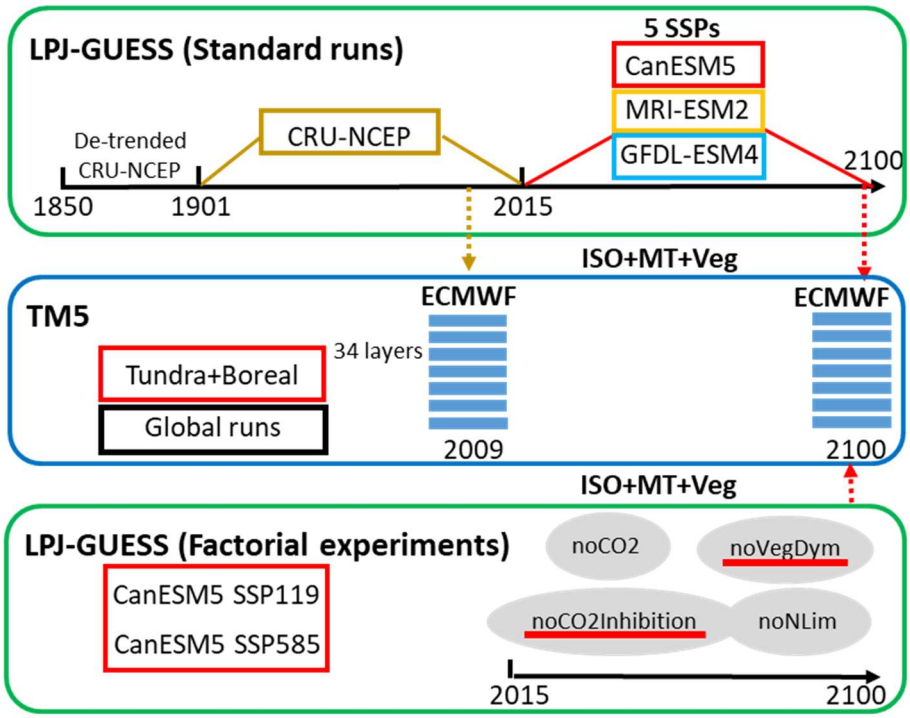

Figure 4 Model setup. The modelled monthly isoprene (ISO) and monoterpene (MT) emissions, as well as vegetation status (Veg) from LPJ-GUESS standard and factorial runs were used as inputs for TM5. The year 2009 and 2100 were selected to represent historical and future periods in the global model TM5. ECMWF: European Centre for Medium-Range Weather Forecasts. SSPs: Shared Socioeconomic Pathways (SSPs).

Global chemistry transport model, TM5

To further assess the impacts of plant-emitted BVOCs on atmospheric aerosols and cloud condensation nuclei (CCN), the modelled leaf area index and vegetation coverage, together with isoprene and monoterpene emissions were fed into a global chemistry transport model, TM5-MP[41]. TM5-MP is a branch of TM5 with a massively parallel functionally and is now maintained by KNMI (Royal Netherlands Meteorological Institute). Throughout the text, we call the model as TM5 for simplicity. The meteorological and surface fields driving the model were derived from ERA-Interim reanalysis datasets provided by ECMWF (European Centre for Medium-range Weather Forecasts)[42], which are he default forcing datasets for TM5. The chemistry scheme used in this study is a modified version of CB05 (carbon bond mechanism; Yarwood, et al. [43]) with more details described in Williams, et al. [41]. Aerosol processes are calculated with the modal two-moment model M7[44]. It includes seven log-normally distributed modes comprising four water-soluble modes (nucleation, Aitken, accumulation and coarse) and three insoluble modes (Aitken, accumulation and coarse). The dry diameter range of each mode is < 10 nm for nucleation mode, 10 nm to 100 nm for Aitken mode, 100 nm to 1000 nm for accumulation mode and > 1000 nm for coarse mode.

Originally in TM5, inputs of monthly mean natural emissions of isoprene and monoterpenes are derived from MEGANv2.1[14,15]. Then a diurnal cycle is applied to the monthly mean values. However, in this study, we substituted these monthly mean emission data by the emission outputs from individual LPJ-GUESS simulation runs. In all the chemistry simulations, the emission data, vegetation status and vegetation coverage south of the study domain were all set to values from the same standard LPJ-GUESS global run from the year 2009 to ensure that changes to the atmospheric chemistry originate from high-latitude changes only. Furthermore, for the year 2100, we used LPJ-GUESS outputs from standard runs of CanESM SSP585 and CanESM SSP119, as well as the outputs from two factorial experiments: noVegDym and noCO2Inhibition, as inputs for TM5. The emissions of isoprene and monoterpenes from biomass burning were applied from the default inventory provided by van Marle, et al. [45] without diurnal variations. Furthermore, the oceanic dimethylsulfide (DMS) emissions, the mineral dust emissions and the sea salt emissions are calculated within TM5[46]. The other natural emissions such as CO, non-methane VOCs, NOx (NO+NO2), NH3 and SO2 were prescribed as in van Noije, et al. [47]. The anthropogenic and biomass burning emissions of gases and particles were derived for present-day conditions from the CMIP6 input4MIPs inventory[45,48].

Once emitted, isoprene and monoterpenes can react with hydroxyl radical (OH) and ozone (O_3) to produce ELVOCs (extreme low volatile organic compounds) and SVOCs (semi-volatile organic compounds), which can condense on particles to increase SOA mass. In addition, ELVOCs can participate in new particle formation together with sulfuric acid. These processes were recently implemented in TM5, which showed better comparison with the observation of aerosol concentration and satellite data of AOD (see Bergman, et al. [28] for more details).

In this study, a horizontal resolution of 3 degrees in longitude and 2 degrees in latitude was applied. In the vertical direction, 34 hybrid-sigma levels were used. The time step was one hour. All the simulations were run for the year 2009 with a spin-up period of one year. The meteorological and surface fields in 2009 were applied for all the simulation cases, which omitted the meteorological impacts in future scenarios when compared to the present case. Similarly, all the emission datasets applied in all the simulation cases were from the year 2009 except those derived from LPJ-GUESS output as mentioned above. TM5 was installed and configured in CSC (Finnish IT Center for Science) Puhti.

Acknowledgement

J.T. is supported by Swedish FORMAS (Forskningsråd för hållbar utveckling) mobility Grant (2016-01580) and European Union's Horizon 2020 research and innovation programme under Marie Sklodowska-Curie Grant 707187. R.R. would like to acknowledge the support by the European Research Council under the European Union's Horizon 2020 research and innovation programme (Grant No 771012). J.T., G.S., and R.R acknowledge the Danish National Research Foundation (CENPERM DNRF100). P. Z. and R. M. would like to acknowledge the funding from EU H2020 project FORCeS (grant agreement No 821205), University of Helsinki Three Year Grant AGES, the ACCC Flagship funded by the Academy of Finland (337549) and CSC (IT Center for Science, Finland) for computational resources. P. Z. also acknowledges the Arctic Avenue (spearhead research project between the University of Helsinki and Stockholm University).

P.A.M. and A.G. acknowledge the Lund University Strategic Research Areas BECC and MERGE for their financial support, and P.A.M. was partly funded by the project BioDiv-Support through the 2017-2018 Belmont Forum and BiodivERsA joint call for research proposals, under the BiodivScen ERA-Net COFUND programme, and with the funding organisations AKA (Academy of Finland contract no 326328), ANR (ANR-18-EBI4-0007), BMBF (KFZ: 01LC1810A), FORMAS (contract no:s 2018-02434, 2018-02436, 2018-02437, 2018-02438) and MICINN (through APCIN: PCI2018-093149).

J.T. would like to thank Roger Seco for providing eddy covariance-based BVOC measurement data from Abisko. All LPJ-GUESS simulations in this paper were performed using Danish e-infrastructure Cooperation (DeiC) National Life Science Supercomputer at Technical University of Denmark. All TM5 simulations in this paper were performed using the Atos Bullsequana X400 supercomputing platform Puhti provided by CSC (IT Center for Science) in Finland.

References

1 Bjorkman, A. D. *et al.* Plant functional trait change across a warming tundra biome. *Nature* **562**, 57-62, doi:10.1038/s41586-018-0563-7 (2018).

2 Myers-Smith, I. H. *et al.* Complexity revealed in the greening of the Arctic. *Nature Climate Change* **10**, 106-117, doi:10.1038/s41558-019-0688-1 (2020).

3 Rinnan, R. *et al.* Separating direct and indirect effects of rising temperatures on biogenic volatile emissions in the Arctic. *Proceedings of the National Academy of Sciences* **117**, 32476-32483, doi:10.1073/pnas.2008901117 (2020).

4 Finger, R. A. *et al.* Effects of permafrost thaw on nitrogen availability and plant–soil interactions in a boreal Alaskan lowland. *Journal of Ecology* **104**, 1542-1554, doi:https://doi.org/10.1111/1365-2745.12639 (2016).

5 Keuper, F. *et al.* A frozen feast: thawing permafrost increases plant-available nitrogen in subarctic peatlands. *Global Change Biology* **18**, 1998-2007, doi:https://doi.org/10.1111/j.1365-2486.2012.02663.x (2012).

6 Possell, M., Nicholas Hewitt, C. & Beerling, D. J. The effects of glacial atmospheric CO2 concentrations and climate on isoprene emissions by vascular plants. *Global Change Biology* **11**, 60-69, doi:https://doi.org/10.1111/j.1365-2486.2004.00889.x (2005).

7 Rosenstiel, T. N., Potosnak, M. J., Griffin, K. L., Fall, R. & Monson, R. K. Increased CO2 uncouples growth from isoprene emission in an agriforest ecosystem. *Nature* **421**, 256-259, doi:10.1038/nature01312 (2003).

8 Peñuelas, J. & Staudt, M. BVOCs and global change. *Trends in Plant Science* **15**, 133-144, doi:https://doi.org/10.1016/j.tplants.2009.12.005 (2010).

9 Atkinson, R. Atmospheric chemistry of VOCs and NOx. *Atmospheric Environment* **34**, 2063-2101, doi:https://doi.org/10.1016/S1352-2310(99)00460-4 (2000).

10 Paasonen, P. *et al.* Warming-induced increase in aerosol number concentration likely to moderate climate change. *Nature Geoscience* **6**, 438-442, doi:10.1038/ngeo1800 (2013).

11 Roldin, P. *et al.* The role of highly oxygenated organic molecules in the Boreal aerosol-cloud-climate system. *Nature Communications* **10**, 4370, doi:10.1038/s41467-019-12338-8 (2019).

12 Schmale, J., Zieger, P. & Ekman, A. M. L. Aerosols in current and future Arctic climate. *Nature Climate Change* **11**, 95-105, doi:10.1038/s41558-020-00969-5 (2021).

13 Mauritsen, T. *et al.* An Arctic CCN-limited cloud-aerosol regime. *Atmos. Chem. Phys.* **11**, 165-173, doi:10.5194/acp-11-165-2011 (2011).

14 Guenther, A. B. *et al.* The Model of Emissions of Gases and Aerosols from Nature version 2.1 (MEGAN2.1): an extended and updated framework for modeling biogenic emissions. *Geosci. Model Dev.* **5**, 1471-1492, doi:10.5194/gmd-5-1471-2012 (2012).

15 Sindelarova, K. *et al.* Global data set of biogenic VOC emissions calculated by the MEGAN model over the last 30 years. *Atmos. Chem. Phys.* **14**, 9317-9341, doi:10.5194/acp-14-9317-2014 (2014).

16 Smith, B. *et al.* Implications of incorporating N cycling and N limitations on primary production in an individual-based dynamic vegetation model. *Biogeosciences* **11**, 2027-2054, doi:10.5194/bg-11-2027-2014 (2014).

17 Tang, J. *et al.* Challenges in modelling isoprene and monoterpene emission dynamics of Arctic plants: a case study from a subarctic tundra heath. *Biogeosciences* **13**, 6651-6667, doi:10.5194/bg-13-6651-2016 (2016).

18 Eyring, V. *et al.* Overview of the Coupled Model Intercomparison Project Phase 6 (CMIP6) experimental design and organization. *Geosci. Model Dev.* **9**, 1937-1958, doi:10.5194/gmd-9-1937-2016 (2016).

19 Dinerstein, E. *et al.* An Ecoregion-Based Approach to Protecting Half the Terrestrial Realm. *BioScience* **67**, 534-545, doi:10.1093/biosci/bix014 (2017).

20 Pearson, R. G. *et al.* Shifts in Arctic vegetation and associated feedbacks under climate change. *Nature Climate Change* **3**, 673-677, doi:10.1038/nclimate1858 (2013).

21 Soja, A. J. *et al.* Climate-induced boreal forest change: Predictions versus current observations. *Global and Planetary Change* **56**, 274-296, doi:https://doi.org/10.1016/j.gloplacha.2006.07.028 (2007).

22 Edwards, M. E., Brubaker, L. B., Lozhkin, A. V. & Anderson, P. M. STRUCTURALLY NOVEL BIOMES: A RESPONSE TO PAST WARMING IN BERINGIA. *Ecology* **86**, 1696-1703, doi:https://doi.org/10.1890/03-0787 (2005).

23 Arneth, A. *et al.* Process-based estimates of terrestrial ecosystem isoprene emissions: incorporating the effects of a direct CO₂-isoprene interaction. *Atmos. Chem. Phys.* **7**, 31-53, doi:10.5194/acp-7-31-2007 (2007).

24 Sporre, M. K., Blichner, S. M., Karset, I. H. H., Makkonen, R. & Berntsen, T. K. BVOC–aerosol–climate feedbacks investigated using NorESM. *Atmos. Chem. Phys.* **19**, 4763-4782, doi:10.5194/acp-19-4763-2019 (2019).

25 Schurgers, G., Arneth, A., Holzinger, R. & Goldstein, A. H. Process-based modelling of biogenic monoterpene emissions combining production and release from storage. *Atmos. Chem. Phys.* **9**, 3409-3423, doi:10.5194/acp-9-3409-2009 (2009).

26 Niinemets, Ü., Tenhunen, J. D., Harley, P. C. & Steinbrecher, R. A model of isoprene emission based on energetic requirements for isoprene synthesis and leaf photosynthetic properties for Liquidambar and Quercus. *Plant Cell Environ* **22**, 1319-1335, doi:https://doi.org/10.1046/j.1365-3040.1999.00505.x (1999).

27 Davies-Barnard, T. *et al.* Nitrogen cycling in CMIP6 land surface models: progress and limitations. *Biogeosciences* **17**, 5129-5148, doi:10.5194/bg-17-5129-2020 (2020).

28 Bergman, T. *et al.* Description and Evaluation of a Secondary Organic Aerosol and New Particle Formation Scheme within TM5-MP v1.1. *Geosci. Model Dev. Discuss.* **2021**, 1-43, doi:10.5194/gmd-2021-49 (2021).

29 Wilkinson, M. J. *et al.* Leaf isoprene emission rate as a function of atmospheric CO2 concentration. *Global Change Biology* **15**, 1189-1200, doi:https://doi.org/10.1111/j.1365-2486.2008.01803.x (2009).

30 Chapin, F. S., 3rd *et al.* Role of land-surface changes in arctic summer warming. *Science* **310**, 657-660, doi:10.1126/science.1117368 (2005).

31 Swann, A. L., Fung, I. Y., Levis, S., Bonan, G. B. & Doney, S. C. Changes in Arctic vegetation amplify high-latitude warming through the greenhouse effect. *Proceedings of the National Academy of Sciences* **107**, 1295-1300, doi:10.1073/pnas.0913846107 (2010).

32 Young, P. J., Arneth, A., Schurgers, G., Zeng, G. & Pyle, J. A. The CO₂ inhibition of terrestrial isoprene emission significantly affects future ozone projections. *Atmos. Chem. Phys.* **9**, 2793-2803, doi:10.5194/acp-9-2793-2009 (2009).

33 Sporre, M. K. *et al.* Large difference in aerosol radiative effects from BVOC-SOA treatment in three Earth system models. *Atmos. Chem. Phys.* **20**, 8953-8973, doi:10.5194/acp-20-8953-2020 (2020).

34 Wania, R., Ross, I. & Prentice, I. C. Integrating peatlands and permafrost into a dynamic global vegetation model: 1. Evaluation and sensitivity of physical land surface processes. *Global Biogeochemical Cycles* **23**, doi:https://doi.org/10.1029/2008GB003412 (2009).

35 Wania, R., Ross, I. & Prentice, I. C. Implementation and evaluation of a new methane model within a dynamic global vegetation model: LPJ-WHyMe v1.3.1. *Geosci. Model Dev.* **3**, 565-584, doi:10.5194/gmd-3-565-2010 (2010).

36 Tang, J. *et al.* Carbon budget estimation of a subarctic catchment using a dynamic ecosystem model at high spatial resolution. *Biogeosciences* **12**, 2791-2808, doi:10.5194/bg-12-2791-2015 (2015).

37 Collatz, G. J., Ball, J. T., Grivet, C. & Berry, J. A. Physiological and environmental regulation of stomatal conductance, photosynthesis and transpiration: a model that includes a laminar boundary layer. *Agricultural and Forest Meteorology* **54**, 107-136, doi:https://doi.org/10.1016/0168-1923(91)90002-8 (1991).

38 Farquhar, G. D., von Caemmerer, S. & Berry, J. A. A biochemical model of photosynthetic CO2 assimilation in leaves of C3 species. *Planta* **149**, 78-90, doi:10.1007/BF00386231 (1980).

39 Viovy, N. (Research Data Archive at the National Center for Atmospheric Research, Computational and Information Systems Laboratory, Boulder, CO, 2018).

40 Ahlström, A., Schurgers, G., Arneth, A. & Smith, B. Robustness and uncertainty in terrestrial ecosystem carbon response to CMIP5 climate change projections. *Environmental Research Letters* **7**, 044008, doi:10.1088/1748-9326/7/4/044008 (2012).

41 Williams, J. E., Boersma, K. F., Le Sager, P. & Verstraeten, W. W. The high-resolution version of TM5-MP for optimized satellite retrievals: description and validation. *Geosci. Model Dev.* **10**, 721-750, doi:10.5194/gmd-10-721-2017 (2017).

42 Dee, D. P. *et al.* The ERA-Interim reanalysis: configuration and performance of the data assimilation system. *Quarterly Journal of the Royal Meteorological Society* **137**, 553-597, doi:https://doi.org/10.1002/qj.828 (2011).

43 Yarwood, G. *et al.* in *9th Annual CMAS Conference* (Chapel Hill, 2010).

44 Vignati, E., Wilson, J. & Stier, P. M7: An efficient size-resolved aerosol microphysics module for large-scale aerosol transport models. *Journal of Geophysical Research: Atmospheres* **109**, doi:https://doi.org/10.1029/2003JD004485 (2004).
45 van Marle, M. J. E. *et al.* Historic global biomass burning emissions for CMIP6 (BB4CMIP) based on merging satellite observations with proxies and fire models (1750–2015). *Geosci. Model Dev.* **10**, 3329-3357, doi:10.5194/gmd-10-3329-2017 (2017).
46 van Noije, T. *et al.* EC-Earth3-AerChem: a global climate model with interactive aerosols and atmospheric chemistry participating in CMIP6. *Geosci. Model Dev.* **14**, 5637-5668, doi:10.5194/gmd-14-5637-2021 (2021).
47 van Noije, T. P. C. *et al.* Simulation of tropospheric chemistry and aerosols with the climate model EC-Earth. *Geosci. Model Dev.* **7**, 2435-2475, doi:10.5194/gmd-7-2435-2014 (2014).
48 Hoesly, R. M. *et al.* Historical (1750–2014) anthropogenic emissions of reactive gases and aerosols from the Community Emissions Data System (CEDS). *Geosci. Model Dev.* **11**, 369-408, doi:10.5194/gmd-11-369-2018 (2018).

Supplementary Files

This is a list of supplementary files associated with this preprint. Click to download.

- ExtendedData.pdf